

A framework for modelling mechanical behavior of surrounding rocks of underground openings under seismic load

Yuting Zhang*, Xiuli Ding, Shuling Huang, Qitao Pei and Yongjin Wu

Key Laboratory of Geotechnical Mechanics and Engineering of the Ministry of Water Resources,
Yangtze River Scientific Research Institute, Wuhan, Hubei 430010, China

(Received February 12, 2017, Revised December 9, 2017, Accepted December 16, 2017)

Abstract. The surrounding rocks of underground openings are natural materials and their mechanical behavior under seismic load is different from traditional man-made materials. This paper proposes a framework to comprehensively model the mechanical behavior of surrounding rocks. Firstly, the effects of seismic load on the surrounding rocks are summarized. Three mechanical effects and the mechanism, including the strengthening effect, the degradation effect, and the relaxation effect, are detailed, respectively. Then, the framework for modelling the mechanical behavior of surrounding rocks are outlined. The strain-dependent characteristics of rocks under seismic load is considered to model the strengthening effect. The damage concept under cyclic load is introduced to model the degradation effect. The quantitative relationship between the damage coefficient and the relaxation zone is established to model the relaxation effect. The major effects caused by seismic load, in this way, are all considered in the proposed framework. Afterwards, an independently developed 3D dynamic FEM analysis code is adopted to include the algorithms and models of the framework. Finally, the proposed framework is illustrated with its application to an underground opening subjected to earthquake impact. The calculation results and post-earthquake survey conclusions are seen to agree well, indicating the effectiveness of the proposed framework. Based on the numerical calculation results, post-earthquake reinforcement measures are suggested.

Keywords: rock material; material strengthening; material degradation; relaxation zone; earthquake effect; numerical analysis

1. Introduction

Rock is a unique natural material that constitutes the primary component of Earth crust. Many rock engineering projects, such as tunnels, underground powerhouses of hydropower plants, and nuclear repositories, are built underground in rocks. Surrounding rock stability of such subsurface openings, especially in high earthquake intensity area, is constantly affected by earthquakes. It is, therefore, necessary to investigate the mechanical behavior of surrounding rocks of underground openings under earthquake effect and to evaluate the potential impact to subsurface structures through proper approaches.

So far, many scholars have conducted researches on related topics and achieved fruitful results. As common types of dynamic loads, the shock wave and explosive wave are frequently studied regarding their transmission characteristics and corresponding dynamic response of structures (Grady 1996, Fattah *et al.* 2012, Mahmoud 2014, Chowdhury *et al.* 2015, Huang *et al.* 2016). A series of tests have been performed to investigate the mechanical behavior of rocks under dynamic loads with intermediate and high stress rate (Shang *et al.* 1998, Xu *et al.* 2005, Zhang and Lu 2009). The strain rate induced by the shock wave and

explosive wave, in these cases, is considerably higher than that by the seismic load. Moreover, the acting load in blasting and shock is imposed at one time with very short duration. Therefore, although there are constitutive models proposed for rocks under blasting and shock effect (Qi *et al.* 2002, Li *et al.* 2006), the mechanical behavior of rocks under earthquake effect is different and requires a suitable model. Under seismic load, the stability of retaining walls and rock slopes is studied (Ismeik and Shaqour 2015, Yang and Pan 2015). Researches on the stability of rock tunnels under seismic load are also reported and the focuses are mainly placed on artificial boundaries (Fu *et al.* 2015, Fattah *et al.* 2015), assessment methods (Zhang *et al.* 2010, Jafarnia and Varzaghani 2016), and influences of specific geological structures (Cui *et al.* 2016).

It should be noted that, the seismic load is a special dynamic load with its unique properties. It externally imposes mechanical excitation on structures and also is a durative load that repeatedly acts on structures for tens of seconds. The rock material, on the one hand, acts as a propagation medium for seismic wave, and on the other hand, is used for subsurface construction. During earthquakes, the rocks surrounding free surfaces of underground openings should withstand repeatedly imposed seismic load to assure structural safety, while the rocks themselves are in return degraded in material properties and bearing capacity. Thus, an overall and in-depth understanding of the influences of seismic load on surrounding rocks of underground openings is crucial for properly modelling the

*Corresponding author, Ph.D.
E-mail: magicdonkey@163.com

Table 1 Classification of common loads based on strain rate

Classification	Strain rate (unit: s^{-1})	Typical Load
Low strain rate	below 10^{-7}	Creep load
	$10^{-7} \sim 10^{-4}$	Creep load and static load
Intermediate strain rate	$10^{-4} \sim 10^2$	Static load and pseudo-dynamic load
High strain rate	$10^2 \sim 10^4$	Dynamic load
	above 10^4	High dynamic load

Note: different literatures may have small variations in the cutoff values of strain rate, but their difference is not significant

mechanical behavior of rocks, so as to provide rational evaluation for pre-earthquake seismic design and post-earthquake reinforcement.

This paper firstly summarizes the effects of seismic load on surrounding rocks of underground openings. Then, a framework for modelling the mechanical behavior of surrounding rocks of underground openings under seismic load is proposed, in which the mentioned major effects of seismic load are all considered. Afterwards, the numerical implementation of the proposed framework is given, in which the adopted constitutive model and iteration algorithm are introduced. Finally, the proposed framework is illustrated with its application to an underground powerhouse located in the epicentral zone of 2008 Wenchuan earthquake. The comparison of observed structural damage in a post-earthquake survey and numerical simulation results indicates that the proposed framework well describes the mechanical behavior of surrounding rocks under seismic load. On this basis, post-earthquake reinforcement strategies are also suggested.

2. Effects of seismic load on surrounding rocks of underground openings

2.1 Overview of the effects of seismic load

Compared with blasting loads, the seismic load has both similar and different characteristics. The similar aspect is that these loads are dynamic loads, the mechanical properties (regarding strength and deformation parameters) of solid materials appear improved under dynamic loads, and this phenomenon can be referred to as strengthening effect. The different aspect is that the action time of seismic load is significantly longer and the load is repeatedly applied. The mechanical properties of solid materials may be gradually lowered under repetitive load, and this phenomenon can be called degradation effect.

The strengthening and degradation effects are the general characteristics of solid materials under seismic load. For the rocks surrounding underground openings, the seismic load will produce a new effect. As the rock mass is affected by the excavation unloading during construction, the integrity and bearing capacity of the rock mass near the excavation face will decrease and a relaxation zone will be formed within this range. Although the relaxation zone is a

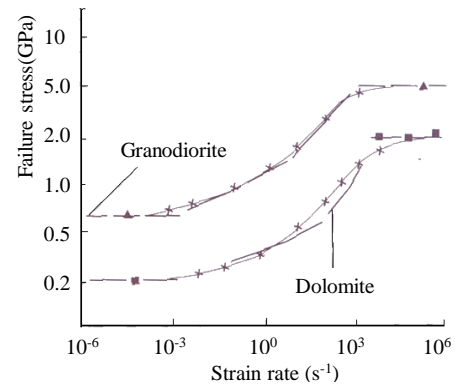


Fig. 1 Mechanical properties under compressive loading with different strain rate

Table 2 Summary of strain rate corresponding to the seismic load

Source	Strain rate (unit: s^{-1})	Target of seismic load
Chen and Li (2003)	$10^{-5} \sim 10^{-1}$	Concrete dam
Bindiganavile (2003)	$5 \times 10^{-3} \sim 5 \times 10^{-1}$	Fiber concrete
Sun and Li (2006)	$10^{-3} \sim 10^{-1}$	Unspecified
Xiao <i>et al.</i> (2001), Xiao <i>et al.</i> (2002), Lin <i>et al.</i> (2003)	$10^{-5} \sim 10^{-2}$	Concrete dam
Zhang (2010)	$10^{-6} \sim 10^{-1}$	Granite rock samples of a hydropower plant

direct result of excavation unloading, the action of seismic load will further aggravate the relaxation of the surrounding rocks, which may lead to further deterioration of the rock mass in the existing relaxation zone and increase its range. Such phenomenon can be called relaxation effect.

The above three effects of seismic load are introduced and their details are as follows.

2.2 Strengthening effect

The strain rate is a measure of the rate of deformation of the material. It is more commonly used for dynamic loads, but in fact applies to all types of loads. According to the magnitude of deformation rate of rock and concrete materials under applied loads, common loads can be classified into different categories as shown in Table 1 (Shang *et al.* 1998, Li *et al.* 2006).

It can be seen from Table 1 that the magnitude of strain rate corresponding to different types of loads is very different. Grady (Grady 1996) performed compressive loading tests on different brittle rock samples (Fig. 1) and found that the failure strength is closely related to the magnitude of strain rate. When the strain rate is small, although the rock strength has increased, the amplitude is not obvious.

Therefore, it is necessary to further find out the magnitude of the strain rate corresponding to the seismic load. Table 2 shows the range of strain rate values for various structures or materials under seismic load, based on the statistics of a number of studies.

It is observed that the strain rate of the structure under the seismic load is roughly in the range of $10^{-6} \sim 10^{-1} s^{-1}$.

However, as the type and material of the objects concerned by different scholars is different, the range of strain rate is different too. This indicates that the magnitude of the strain rate of the structure is not only related to the seismic load, but also to the properties of studied object and its surrounding environment. As there is a large difference in the environment between the underground buildings and the surface buildings, the strain rate of the surrounding rocks of underground openings under the seismic load should be further determined to provide a rational basis for quantitative consideration of the strengthening effect. This issue will be looked into in the framework introduction.

2.3 Degradation effect

Analysis on a large number of measured ground acceleration data reveals that seismic wave can be equivalent to superposition result of multiple simple harmonic curves with different frequencies and amplitudes. During earthquake process, the rock medium withstands random vibration lasting tens of seconds and causes repeated loading and unloading effect to surrounding rocks. This effect is cyclic and may trigger gradual degradation of material properties and cause fatigue failure of surrounding rocks.

Studies (Ge *et al.* 2010) indicates that there is a threshold value determining the initiation of degradation. When amplitude of cyclic load is smaller than the threshold value, the rock properties are generally unaffected and the irreversible deformation is very small. When the amplitude exceeds the threshold value, the number of cycles of cyclic load causes gradually accelerated increase of irreversible deformation and finally leads to the fatigue failure of rock. The threshold value, according to statistics of experimental data, is slightly below the yield value of rock sample in conventional tri-axial test.

For mesoscopic of view, there are many tiny protosomatic fissures and voids in rocks. When the amplitude of externally applied load is low, fissures and voids can maintain their original state. The rocks are only slightly affected and show stable response. When the amplitude exceeds the threshold value, fissures and voids cannot restore their original state when the load is removed and the residual deformation is produced. As the number of cyclic load increases, the residual deformation gradually accumulates. During this process, tiny cracks are initiated, growing larger and contributing to the generation of macro-cracks, thus causing the fatigue failure of rock. The degradation process of rock under externally applied load can be generalized as a result of initiation, growth, and connection of cracks. As this process is closely associated with cracks, the proposed framework introduces the damage concept as an indicator for material property degradation quantifications.

2.4 Relaxation effect

The surrounding rocks of underground openings are disturbed by the excavation unloading and the redistribution of geo-stress, thus causing adverse effect to rock mass properties and then generating relaxation zone. Fig. 2 plots

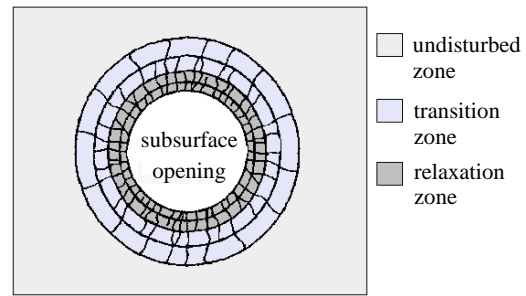


Fig. 2 Relaxation zone of surrounding rocks

Table 3 Effects of seismic load and their mechanisms

Effects	Mechanisms	Inclusion of the effects in the framework
Strengthening	Increase mechanical properties of rocks in terms of strength and stiffness parameters	Determine the strain rate of surrounding rocks firstly and then the increasing extent
Degradation	Tiny cracks grow and irreversible deformation accumulates under cyclic load, causing fatigue failure.	Use the damage concept for degradation quantifications of surrounding rocks
Relaxation	Tiny cracks grow, develop into macro-cracks after excavation, and are further degraded under seismic wave stress.	Determine the range of relaxation zone under seismic load to provide bases for post-earthquake reinforcement

the relaxation zone and the classification of its adjacent area. Due to excavation effect, tiny cracks inside rock develop into macro-cracks and form the relaxation zone. Evaluation result of relaxation zone scale is a crucial index for anchor support design. The acoustic emission method is always used to assess the quality of rock mass subjected to blasting.

During earthquake process, the transmission of seismic action produces stress fluctuations in the rock medium and the stress is amplified near the free surfaces of underground openings. Thus, although the surrounding rocks within the relaxation zone are reinforced after excavation and have a certain bearing capacity, they are still degraded under seismic load and most prone to damage. The evaluation result of relaxation zone after earthquake, in this case, is also an essential index for post-earthquake restoration and reinforcement. The relaxation effect, which is commonly used in rock mass stability evaluation under excavation unloading, can be also used to evaluate the influences of seismic load.

3. Framework for modelling mechanical behavior of surrounding rocks under seismic load

3.1 Outline of the framework

The effects of seismic load on surrounding rocks and their mechanism are detailed above. Table 3 summarizes the mechanisms of the effects briefly and introduces how they will be included in the proposed framework.

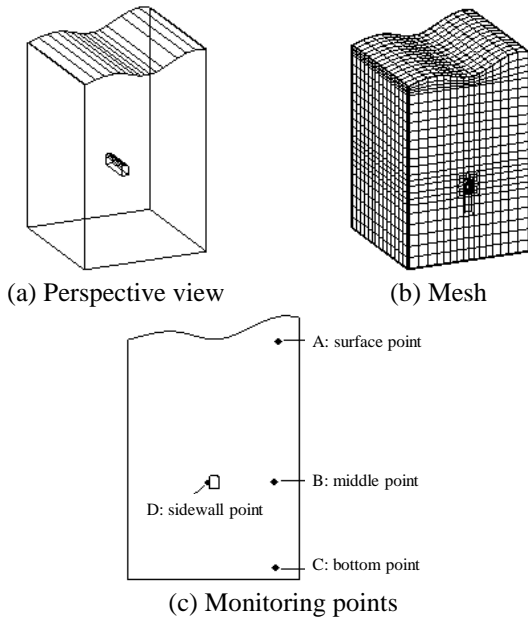


Fig. 3 Calculation model for determination of the strain rate of surrounding rocks

3.2 Modelling the strengthening effect

3.2.1 Strain rate of surrounding rocks of underground openings under seismic load

To determine the general range of strain rate of surrounding rocks under seismic load, an independently developed 3D elastic dynamic FEM analysis code (Zhang 2011) is adopted. The dynamic responses of surrounding rocks of underground openings under seismic load are calculated, and the magnitude of the strain rate distribution of surrounding rocks are obtained.

An underground cavern model is created, as shown in Fig. 3. It contains a total of 8,416 hexahedral elements and 9,738 nodes. The length, width and height of the model are 350 m×350 m×550 m and a long-shaped cavern with its length × width × height of 100 m×20 m×30 m is considered inside. The equivalent viscoelastic boundary element (Liu *et al* 2007) is adopted as the artificial boundary. Four monitoring points are set to obtain the strain rate distribution law. These points are located at the top, the middle, the bottom of the model, and the sidewall area of the surrounding rocks, respectively. The deformation modulus is 10 GPa and the Poisson's ratio is 0.30. The EL-Centro acceleration record (Fig. 4) is used as input seismic effect. The amplitude of input acceleration record is adjusted to 3.0 m/s². The seismic waves are considered vertically incident from the bottom of the model in terms of *P* wave and *S* wave.

The strain rate tensor $\dot{\epsilon}_{ij}$ can be calculated by

$$\dot{\epsilon}_{ij} = \frac{1}{2}(v_{i,j} + v_{j,i}) \quad (1)$$

where $v_{i,j}$ is the tensor of velocity field. Then the equivalent strain rate $\dot{\bar{\epsilon}}$ is obtained using

$$\dot{\bar{\epsilon}} = \sqrt{\frac{2}{3}\dot{\epsilon}_{ij}\dot{\epsilon}_{ij}} \quad (2)$$

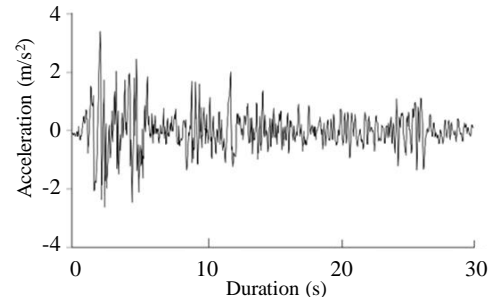


Fig. 4 El-centro acceleration record

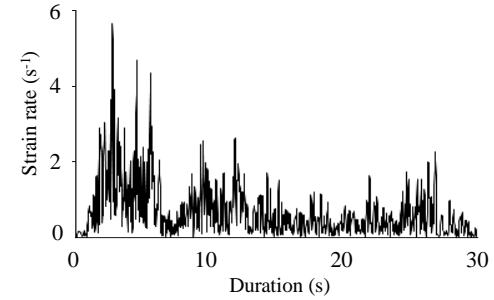


Fig. 5 Equivalent strain rate for point D

Table 4 Distribution of equivalent strain rate values for the four monitoring points

Ranges of value $\dot{\bar{\epsilon}}$	A	B	C	D
$10^{-3} \text{ s}^{-1} \sim 10^{-2} \text{ s}^{-1}$	7.74%	13.61%	16.01%	21.28%
$10^{-4} \text{ s}^{-1} \sim 10^{-3} \text{ s}^{-1}$	76.92%	73.52%	75.98%	70.11%
$10^{-4} \text{ s}^{-1} \sim 10^{-5} \text{ s}^{-1}$	14.34%	12.21%	7.81%	7.87%
$< 10^{-5} \text{ s}^{-1}$	1.00%	0.66%	0.20%	0.74%

The calculated equivalent strain rate for monitoring point *D* is plotted (Fig. 5). The curve of equivalent strain rate versus calculation duration is consistent with the input acceleration record and the maximum value is $5.66 \times 10^{-3} \text{ s}^{-1}$. Table 4 summarizes the distribution of equivalent strain rate values for the considered monitoring points and following findings can be noted.

(1) The maximum values of strain rate for monitoring points *A*, *B*, and *C* are $4.65 \times 10^{-3} \text{ s}^{-1}$, $5.11 \times 10^{-3} \text{ s}^{-1}$, and $4.54 \times 10^{-3} \text{ s}^{-1}$, respectively. This indicates that variation trend of the amplitudes of strain rate as the depth varies is not remarkable.

(2) The monitoring points *B* and *D* are located at the same depth. But the maximum value of strain rate at point *D* is about 20% larger than the value at point *B*, showing that the free surfaces of underground openings has an amplification effect on the strain rate.

(3) The distribution of equivalent strain rate values for the four monitoring points is similar. The strain rate values in the whole calculation duration are smaller than $1 \times 10^{-2} \text{ s}^{-1}$ and most values distribute in the order of 10^{-5} to 10^{-3} .

Sensitivity analysis is further done to investigate the influences of material properties and seismic intensity on the strain rate values. Firstly, the deformation modulus adopts 20 GPa, 30 GPa, and 40 GPa to perform analyses, respectively by using the original seismic input parameters. Then, the deformation modulus is restored to 10 GPa and

the amplitude of input acceleration record data are reduced by half (1.5 m/s^2) and increased by half (4.5 m/s^2), respectively to perform analyses. The obtained results indicate that the findings on the strain rate value distribution is still valid. Combining Table 2, it is concluded that the strain rate values of surrounding rocks of underground openings under seismic load are at least one order of magnitude lower than the strain rate values of concrete dams.

3.2.2 Consideration of strain-dependent characteristics

The strengthening effect of seismic load leads to the increase of mechanical properties of surrounding rocks. For strength parameters of rock, researches (Chong *et al.* 1980, Ju and Wu 1993) indicated that both compressive and tensile strengths increase as the strain rate increases, but the increasing extents are different depending on specific rock type and confining pressure. Eq. (3) describes the variation of strength parameters under dynamic loads

$$f_d = g(\dot{\epsilon}) f_s \quad (3)$$

where f_d is the strength under dynamic load (also dynamic strength), f_s is the static strength obtained by conventional tests, $\dot{\epsilon}$ is the strain rate, and $g(\dot{\epsilon})$ is a strain rate dependent function describing the variation of dynamic strength compared to the static strength. Due to the complicated nature of rock material, $g(\dot{\epsilon})$ may vary as the lithological and environmental conditions change, and till now there is no widely accepted quantitative expressions for $g(\dot{\epsilon})$.

The Euro-International Committee for Concrete (CEB) recommended $g(\dot{\epsilon})$ for concrete as

$$g(\dot{\epsilon}) = (\dot{\epsilon}_d / \dot{\epsilon}_s)^{1.026\alpha} \quad (4)$$

where $\dot{\epsilon}_s$ equals to $3 \times 10^{-6} \text{ s}^{-1}$ and is viewed as the strain rate under static condition. $\dot{\epsilon}_d$ is the dynamic strain rate ranging from $3 \times 10^{-6} \text{ s}^{-1}$ to 30 s^{-1} . $g(\dot{\epsilon})$ is the expression describing the quantitative relationships between the static strength and the dynamic strength under compressive condition. $\alpha = (5 + 3f_{cu}/4)^{-1}$, f_{cu} is the static compressive strength for cubic concrete sample and its unit is MPa. By substituting the maximum and minimum values of the strain rate of surrounding rocks under seismic load into Eq. (4), the distribution of $g(\dot{\epsilon})$ can be obtained considering different compressive strength values of rocks. It is observed that (Fig. 6), the increase of strength parameter is gradually reduced with the increase of static compressive strength, indicating that the strengthening effect is more significant for soft rocks than hard rocks. To further determine the variation of Mohr-Coulomb shear parameters, the Mohr circle regarding the uniaxial compressive tests is used (Fig. 7). It provides a relationship between the cohesion value c and the maximum principal stress σ_1 as

$$c = \frac{\sigma_1 \cos \varphi}{2(1 + \sin \varphi)} = \frac{R_c \cos \varphi}{2(1 + \sin \varphi)} \quad (5)$$

where R_c is the compressive strength of rock and φ is the internal frictional angle. It should be noted that, Eq. (5) is only a rough estimation based on the assumptions that the strength envelope line is straight. The Mohr-Coulomb shear parameters obtained from shear tests are commonly used. Despite this, Eq. (5) provides a quantitative relation. Li

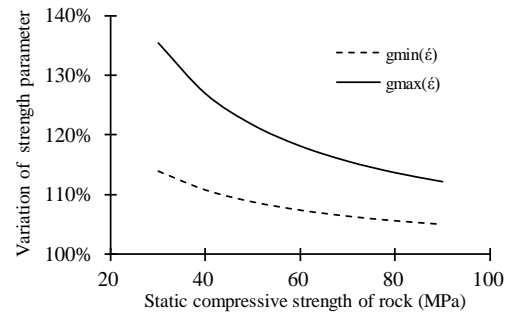


Fig. 6 Variation of strength parameter with different compressive strength values of rocks

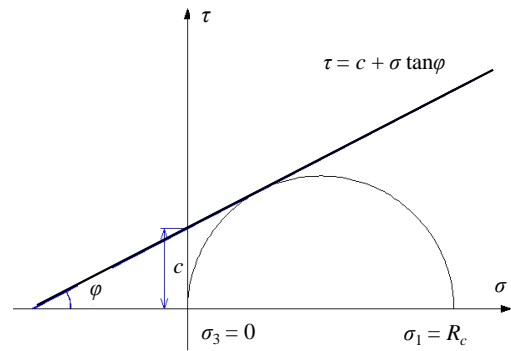


Fig. 7 Mohr circle corresponding to the uniaxial compressive test of rocks

(2007) pointed out that the variation of internal frictional angle under dynamic load is very small as below

$$\varphi_d \approx \varphi \quad (6)$$

where φ_d is the internal frictional angle under dynamic load. So the cohesion value c can be considered in rough linear relation to the compressive strength. Therefore, the Eq. (4) is adopted in the framework to describe the variation of strength and shear parameters of surrounding rocks.

For deformation parameter of rocks, Eq. (7) describes its variation under dynamic loads

$$E_d = h(\dot{\epsilon}) E_s \quad (7)$$

where E_d is the deformation modulus under dynamic load (also dynamic deformation modulus), E_s is the static deformation modulus, $\dot{\epsilon}$ is the strain rate, and $h(\dot{\epsilon})$ is a strain rate dependent function describing the variation of dynamic modulus compared to static modulus. Reports on the change of deformation parameters of rocks under seismic load are rare. The experimental data show that the difference of the dam concrete dynamic and static elastic modulus values are not considerable (The Professional Standards Compilation Group of the People's Republic of China 2015). As the rock material is far more complex than the concrete, $h(\dot{\epsilon})$ is assigned the value of 1.0 in the framework to provide a sufficient safety margin. That is, the strengthening effect on deformation parameter of rocks is not considered.

3.3 Modelling the degradation effect

3.3.1 Generalization of rock degradation under seismic load

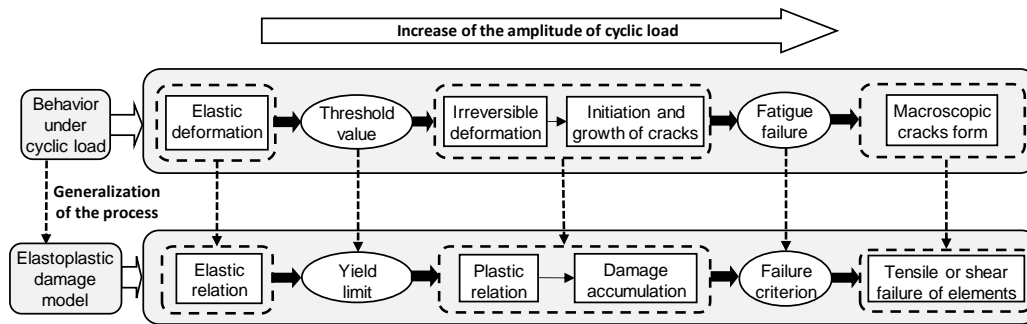


Fig. 8 Generalization of mechanical behavior of rocks under cyclic load using elastoplastic damage model

The degradation of surrounding rocks under seismic load can be generalized as the material degradation subjected the cyclic load. Irreversible deformation is produced and accumulated when the cyclic load exceeds a certain threshold value. The damage concept is suitable for describing the degradation process because the behavior of cracks is closed related. Based on these understandings, an elastoplastic damage model is considered in the framework to generalize the rock degradation under seismic load (Fig. 8). As can be seen, all of the characteristics of material fatigue failure under cyclic load correspond to the details of the elastoplastic damage model. The following focuses on the concept of material damage and its application in the degradation of rocks under cyclic load. Other problems associated with the constitutive model will be described later in the numerical implementations section.

3.3.2 Definition of material degradation under cyclic load

The concept of damage is defined as material degradation caused by mesoscopic structural defects under external load. The behavior of cracks in rock are in accord with this concept, so degradation of rock can be quantified by using the damage concept. With the progressive failure of rocks, the strain gradually accumulates. When strain exceeds its limit, the rock damage, denoted as D and named as damage coefficient, initiates and develops in positive correlation as

$$D = f(\varepsilon) \quad (\varepsilon > [\varepsilon]) \quad (8)$$

where $[\varepsilon]$ is strain limit. When $\varepsilon < [\varepsilon]$, rock damage does not occur and $D=0$. D in one dimensional cases can be described using uniaxial strain as

$$D = 1 - (\varepsilon_0/\varepsilon)^2 \quad (\varepsilon > [\varepsilon]) \quad (9)$$

where ε_0 is a threshold value determining the start of damage and $[\varepsilon]$ is critical strain and usually corresponds to ultimate tensile strength.

The elastic deformation is reversible and does not produce damage. When hydrostatic pressure is applied, damage does not occur, either. The damage mainly depends on the partial tensor of plastic strain ε_{ij}^p . When damage initiates, its degradation effect on rock properties is a gradually accelerated process. The stress and mechanical parameters of surrounding rocks decrease with the increase of cumulative plastic strain, while the damage coefficient increases with the increase of cumulative plastic deformation.

When the surrounding rocks are close to the ultimate strength, the internal cracks develop rapidly and the damage coefficient increases significantly. The variation of cumulative damage can be described by exponential function. Therefore, the evolution equation for rock damage in 3D condition can be expressed as

$$D = 1 - \exp(-Re_D) \quad (10)$$

where $e_D = \sqrt{e_{ij}^p \cdot e_{ij}^p}$ and R is damage constant. The degradation of rocks mainly affects the deformation parameters. The deformation modulus of rocks under damage state can be valued using

$$E_1 = (1 - D) E \quad (11)$$

where E_1 is the deformation modulus under damage state and E is the original modulus.

3.4 Modelling the relaxation effect

3.4.1 Basic ideas

Usually, based on the results of acoustic emission test, the area where the wave velocity is obviously decreased is defined as the relaxation zone. Due to the excavation unloading and the seismic effect, the integrity of the rock mass within the relaxation zone is greatly affected, leading to the initiation and development of cracks and making the stiffness of rock mass reduced significantly. As the reduction of material stiffness is measured by the damage coefficient based on Eq. (11), the relationship between the relaxation zone of surrounding rocks and the damage coefficient can be established. By using this connection, derivation can be performed and engineering experience can be also combined to obtain their quantitative relationship. That is, the threshold value of damage coefficient can be determined using the proposed framework. The area whose damage coefficient exceeds the threshold value is considered a relaxation zone. The detailed ideas are further illustrated (Fig. 9).

3.4.2 Determination relaxation range of surrounding rocks using damage coefficient

The relaxation range of surrounding rocks is determined based on the AE test results, which mainly contains the variation of longitudinal wave velocity at different depth of rock mass. The elastic modulus, the Poisson's ratio, and the density of propagation medium together determine the

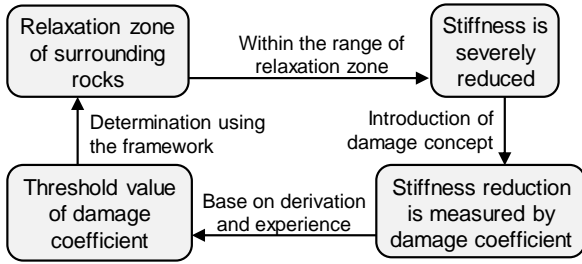


Fig. 9 Relationship between relaxation zone and damage coefficient

longitudinal wave velocity as

$$C_p = \sqrt{\frac{E(1-\mu)}{\rho(1+\mu)(1-2\mu)}} \quad C_{p1} = \sqrt{\frac{E_1(1-\mu)}{\rho_1(1+\mu)(1-2\mu)}} \quad (12)$$

where C_p and C_{p1} are wave velocities for original rock medium and relaxed rock medium, respectively. Divide C_p by C_{p1} , we have

$$\frac{C_{p1}}{C_p} = \sqrt{\frac{\rho E_1}{\rho_1 E}} \quad (13)$$

Combine (11) and (13), we have

$$D = 1 - \frac{E_1}{E} = 1 - \frac{\rho_1}{\rho} \left(\frac{C_{p1}}{C_p} \right)^2 \quad (14)$$

where ρ and ρ_1 are densities. As the volumetric strain θ is defines as

$$\theta = (V_1 - V) / V = \rho / \rho_1 - 1 \quad (15)$$

where V_1 and V are volumes, it also can be calculated by

$$\theta = \varepsilon_1 + \varepsilon_2 + \varepsilon_3 \quad (16)$$

where ε_1 , ε_2 , and ε_3 are the three principal strains. Put (15) into (14), we have

$$D = 1 - \frac{1}{1+\theta} \left(\frac{C_{p1}}{C_p} \right)^2 \quad (17)$$

According to engineering practices and the Chinese national codes regarding evaluation of rock mass quality, it is widely accepted that the surrounding rocks can be judged as relaxation zone where the decreasing extent of longitudinal wave reaches 10%. Therefore, (17) is simplified as

$$[D] \geq 1 - 0.81 (1+\theta)^{-1} \quad (18)$$

If volumetric variation is not considered, then $\theta=0$ and (15) is further written as

$$[D] \geq 0.19 \quad (19)$$

Based on (18) or (19), it is concluded that if the damage coefficient of an element exceeds certain magnitude, then this element is judged within relaxation zone. This magnitude of damage coefficient is the threshold value.

4. Numerical implementations

4.1 Constitutive model

For geo-materials, the Zienkiewicz-Pande criterion uses a hyperbolic yield function to approximate the straight line of the Mohr-Coulomb criterion on the meridional plane and it is adopted

$$F = \sqrt{-\alpha} \left(\sigma_m + \frac{\beta}{2\alpha} \right) + \sqrt{(\bar{\sigma}^2 + \gamma - \frac{\beta^2}{4\alpha})} \quad (20)$$

where $\alpha = -\sin^2\varphi$, $\beta = 2c\sin\varphi\cos\varphi$, $\gamma = a^2\sin^2\varphi - c^2\cos^2\varphi$. $\sigma_m = (\sigma_1 + \sigma_2 + \sigma_3)/3$. Among these parameters, c is cohesion, φ is internal friction angle, and a is a coefficient that describes the approaching extent of yield surface.

When the damage coefficient D is considered, the increment of differential stress is written as

$$\sigma_{ij}^D = (1-D)\sigma_{ij} + \frac{D}{3}\sigma_{kk}\delta_{ij} \quad (21)$$

where is stress tensor σ_{ij}^D considering damage and δ_{ij} is the Kronecker function (also known as Kronecker delta).

The differential form of stress tensor σ_{ij} with regard to strain tensor ε_{ij} is written as

$$d\sigma_{ij} = ([D_e] - [D_p])d\varepsilon_{ij} \quad (22)$$

where $[D_e]$ and $[D_p]$ are elastic and plastic stress matrixes, respectively. Perform differential calculation on (21) according to (22), we have

$$d\sigma_{ij}^D = (1-D)[D_{ep}]d\varepsilon_{ij} + \frac{D}{3}[D_{ep}]d\varepsilon_{ij} - S_{ij}dD \quad (23)$$

If incremental load with each calculation step is sufficiently small, then the damage coefficient D can be viewed as constant during current step and $dD=0$. So (23) can be simplified and further written as

$$d\sigma_{ij}^D = (1-D)[D_{ep}]d\varepsilon_{ij} + \frac{1}{3}D[D_{ep}]d\varepsilon_{ij} = ([H_e] - [H_d])d\varepsilon_{ij} \quad (24)$$

where $[H_e]=[D_e]$ and $[H_d]$ is stress matrix considering damage as

$$[H_d] = (1-D + \frac{D}{3}\delta_{ij})[D_p] + (D - \frac{D}{3}\delta_{ij})[D_e] \quad (25)$$

4.2 Iteration algorithms

The Newmark implicit method is adopted to solve motion equations. Within each step, the non-linear equations are

$$[\bar{K}(\{\delta_t\})]\{\delta_t\} = \{\bar{P}_t\} \quad (26)$$

where $\{\bar{P}_t\}$ is equivalent load. $[\bar{K}(\{\delta_t\})]$ is the equivalent stiffness matrix and is calculated using

$$[\bar{K}(\{\delta_t\})] = [K(\{\delta_t\})] + a_0[M] + a_1[C] \quad (27)$$

where $K(\{\delta_t\})$ is the stiffness matrix which is related to the displacement at t moment, $[M]$ is the mass matrix, and $[C]$ is the damping matrix. a_0 and a_1 are coefficients determined by Newmark method.

As the equivalent stiffness matrix $[\bar{K}(\{\delta_t\})]$ is dependent

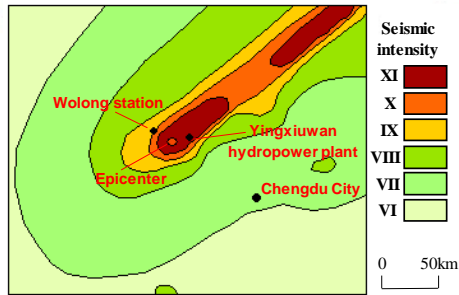


Fig. 10 Location of Yingxiuwan hydropower plant



Fig. 11 Seismic damage of ground structures

on the current displacement information, Eq. (26) should be solve using iteration method. Therefore, the incremental variable plastic stiffness matrix iteration method (Xiao 2000) is adopted. It has fast calculation speed and good convergence. The basic idea of the iteration method is to divide the considered load into elastic part and plastic part. The elastic part of load is applied at one time because the induced deformation is linearly related. The plastic part is further divided into several smaller parts. When the elastic part is applied, the structure immediately comes to the critical state. Then the plastic part is applied by several smaller parts. In each stage of the smaller plastic part, by the plastic stiffness remains unchangeable, the computation process can be accelerated. Each smaller part of plastic load is applied using

$$[K_e]\{\delta_n\}_i = \{\Delta R_p\}_i + [K_p]\{\delta_{n-1}\}_i \quad (28)$$

where $[K_e]$ and $[K_p]$ are the elastic stiffness matrix and plastic stiffness matrix; $\{\delta_n\}_i$ and $\{\delta_{n-1}\}_i$ are displacement increments of current stage and last stage respectively.

5. Case study

5.1 Overview

5.1.1 Basic information of the studied project

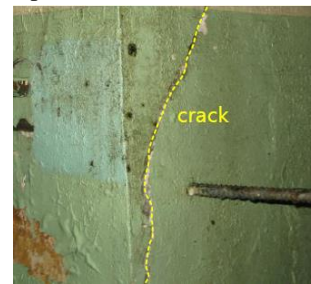
The Yingxiuwan hydropower plant is the nearest hydropower plant to the epicenter of 2008 Wenchuan earthquake (Fig. 10). The power station is one of the nine cascaded hydropower plants on the Minjiang River. The geological exploration work began in 1964 and this plant was put into operation in 1971. The major structures include the underground powerhouse with a buried depth of about 150~250 m, the transformer hall, the bus bar opening, the headrace tunnels, the tailrace tunnels, and the traffic tunnel. The size of the powerhouse is 52.8 m×17.0 m×37.2 m (length×width×height), and the size of the transformer hall is 59.4 m×7.2 m×27.9 m. All of the caverns are excavated in granite and granodiorite. The power plant has been put into operation for many years when the earthquake took place and was seriously affected. The seismic intensity amounts to XI degree for the project site.

5.1.2 Post-earthquake survey on seismic damage

As the nearest hydropower plant to the epicenter, the Yingxiuwan hydropower plant has experienced a “prototype



(a) Underground powerhouse (b) Crack in the traffic tunnel



(c) Crack at tunnel intersection area

Fig. 12 Damage of underground openings subjected to 2008 Wenchuan earthquake

failure test” in the Wenchuan earthquake. Therefore, the buildings and structures of the power plants affected by the impact of the earthquake are the most representative. The post-earthquake investigation was carried out in July 2008, two months after the earthquake. At that time, the restoration and reinforcement work of the hydropower plant had not yet begun, so that the original damage can be investigated and the first-hand damage data can be obtained. According to the survey, it can be found that the ground buildings were severely affected by the earthquake and the seismic damage is serious (Fig. 11).

The seismic damage of underground structures, in comparison, was much better (Fig. 12). There were no block falls and local collapse, and other serious damage. The main powerhouse was basically in good condition. The main form of the earthquake damage is the locally distributed cracks. They were mainly found at the tunnel intersection area and the sidewall area. Although the cracks were found widely distributed, the overall stability of the underground caverns was not affected, indicating that the anti-seismic capacity of underground structures is much stronger than that of the surface structures.

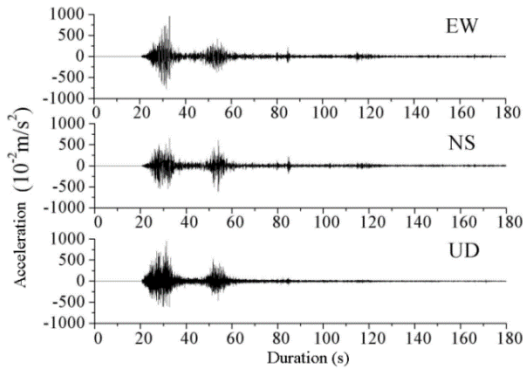


Fig. 13 Measured acceleration time history of main shock at Wolong station

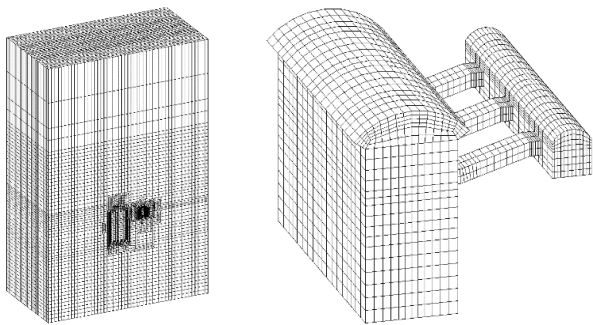


Fig. 14 Calculation mesh model

5.1.3 Characteristics of recorded ground motion

The Wolong station is only 19 km from the 2008 Wenchuan earthquake epicenter (Fig. 10) and it is the nearest one among the strong motion observation stations in the epicentral region. It also measured the maximum peak acceleration. Fig. 13 shows the acceleration time history recorded by Wolong station at the time of the Wenchuan main shock on May 12, 2008, with a sampling frequency of 200 Hz and a continuous recording time of 180 s. The acceleration record is composed of the data in the EW, NS, and UD directions. The peak acceleration for EW, NS, and UD directions is 9.58 m/s², 6.53 m/s², and 9.48 m/s², respectively.

5.2 Numerical analysis of surrounding rock stability using the proposed framework

5.2.1 General procedures

The proposed framework is used to simulate the mechanical behavior of surrounding rocks under seismic effect. Finite element mesh is discretized with 138480 elements and 146475 nodes (Fig. 14). The dimension of the mesh is 200 m×100 m×300m (length×width×height). The strong motion data recorded during the earthquake is used. Note that the duration is 180 s, the data corresponding to the time period of 20 s to 80 s is truncated and used as seismic input.

As the overburden depth of underground opening exceeds 150 m, the seismic input is then cut in half to meet the needs of national codes. The mechanical properties of rock masses are valued as: deformation modulus 10 GPa,

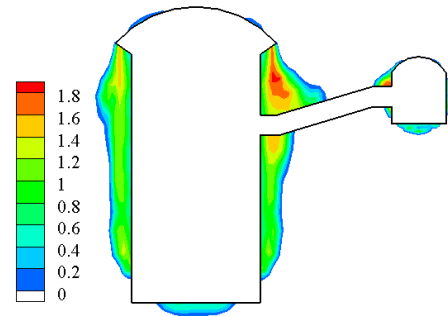


Fig. 15 Color map of envelope value for tensile stress of surrounding rocks (MPa)

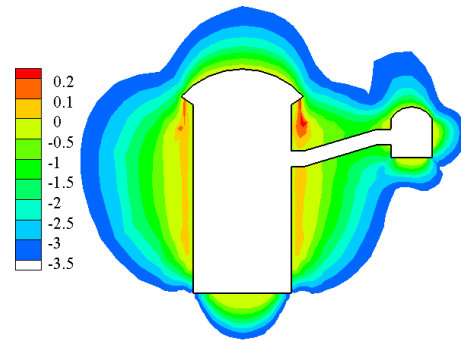


Fig. 16 Color map of the third principal stress (σ_3) of surrounding rocks after earthquake (MPa)

Poisson’s ratio 0.25, cohesion 2.18 MPa, internal friction angle 41.6°, tensile strength 1.97 MPa and bulk density 27.6 kN.m³. These parameters are static ones used in the excavation calculation that is firstly conducted prior to seismic analysis. Then, the strengthening effect of seismic load on mechanical properties is considered and the time history method is conducted.

5.2.2 Calculation results

The color maps of the envelope value for tensile stress and the third principal stress after earthquake calculation are given (Fig. 15 and Fig. 16). It is observed that the distribution of envelope value for tensile stress characteristically shows the location of surrounding rocks where is more likely affected by the tensile effect. The maximum tensile stress reaches the tensile strength of rock mass. In the process of seismic action, the maximum depth of rock mass subjected to tensile effect is about 4.0 m. After the earthquake action, the range of tensile stress area is considerably reduced and the maximum depth is about 2.5 m (Fig. 16). The tensile stress area mainly distributes at the sidewall areas and the tunnel intersection areas. This agrees with real situation and suggests that the obtained result is reliable.

When the seismic input is imposed with considered amplitude, it is found that, in addition to the relaxation zone generated by excavation calculation, there is no new relaxation zone after earthquake calculation. This indicates that the surrounding rocks of Yingxiuwan hydropower plant is still stable. To verify the effectiveness of the proposed framework, the seismic input is then amplified by 20% to re-conduct the time history calculation.

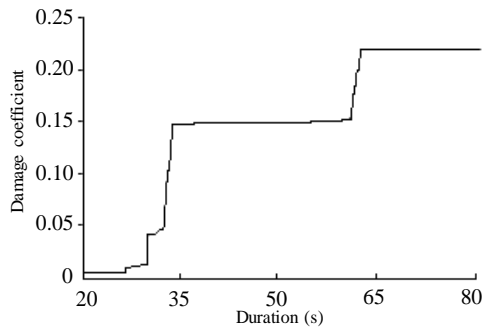


Fig. 17 Time history curve of damage coefficient of an element in the relaxation zone

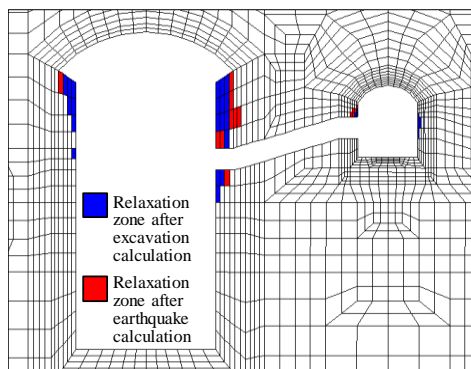


Fig. 18 Distribution of relaxation zone caused by excavation and earthquake effects

The variation of damage coefficient of an element during earthquake calculation is given (Fig. 17). It can be seen that at the start of earthquake calculation, the damage coefficient of this element is very small, indicating the degradation of rock mass caused by excavation unloading is not considerable. However, when the seismic load is applied, the damage coefficient has experienced several significant jumping growth and finally has finally stabilized at the value of 0.22, indicating that this element is considered relaxed based on Eq. (18).

The distribution of the relaxation zone caused by the excavation and the earthquake effect is given (Fig. 18). It is found that by considering the amplified seismic input, there is an increase of the range of relaxation zone of surrounding rocks. It is discovered that relaxation zone mainly distribute at the sidewalls and the tunnel intersection areas, which are same as maximum tensile stress distribution. This coincidence shows that, if seismic impact becomes larger, then cracks grow and develop into macro instability problem. So relaxation zone can be viewed as a subsequent potential failure for rockmass.

5.3 Recommendations for post-earthquake reinforcement

Based on the calculation results, following findings can be of assistance to the consideration of post-earthquake reinforcement work.

(1) The maximum range of tensile stress of the surrounding rocks is about 4.0m during the earthquake, leading to a potential failure such as cracks. Therefore,

measures should be considered to prevent rock mass from the adverse tensile effect caused by seismic load.

(2) Under the original seismic input, there is no new relaxation zone. However, when the input seismic load is amplified to a certain extent, there is an increase of the relaxation zone, which increases the range of relaxation zone. Due to the uncertainties of earthquake action, a certain safety margin should be considered in the reinforcement design.

The post-earthquake reinforcement design, based on the above suggestions, includes such major contents as: (1). Perform pressure grouting on the existing cracks; (2). Install new anchor bolts at the relaxation zones and crack areas. The bolting length, by considering a certain safety reserve, is 6 m.

6. Conclusions

A framework for modelling the mechanical behavior of the surrounding rocks of underground openings under seismic load is proposed. The major mechanical effects induced by earthquake actions, such as the strength effect, the degradation effect, and the relaxation effect, are summarized and the corresponding mechanisms are also detailed. The proposed framework is able to include the above effects by considering the strain-dependent characteristic, by introducing the damage concept, and by using the quantitative relationship between the damage coefficient and the relaxation zone. By incorporating the proposed framework to an independently developed 3D dynamic FEM analysis code, the numerical analysis function is realized. The case study on the underground caverns of Yingxiuwan hydropower plant subjected to the 2008 Wenchuan earthquake shows that the proposed framework is reliable and effective, providing a reliable approach for evaluating the performance of surrounding rocks of underground openings under earthquake impact.

Acknowledgements

Financial supports from the National Key Research and Development Program of China (No. 2016YFC0402008), the National Natural Science Foundation of China (Nos. 51539002, 51779018, 51609018), and the Basic Research Fund for Central Research Institutes of Public Causes (No. CKSF2017054/YT) are greatly acknowledged.

References

- Bindiganavile, V.S. (2003), "Dynamic fracture toughness of fiber reinforced concrete", Ph.D. Dissertation of University of British Columbia, Vancouver, Canada.
- Chen, J.Y. and Li, J. (2003), "Seismic response analysis of high arch dam based on strain rate-dependent concrete damage model", *China Civil Eng. J.*, **36**(10), 46-50.
- Chong, K.P., Hoyt, P.M., Smith, J.W. and Paulsen, B.Y. (1980), "Effects of strain rate on oil shale fracturing", *Int. J. Rock Mech. Min. Sci.*, **17**(1), 35-43.
- Chowdhury, S.S., Deb, K. and Sengupta, A. (2015), "Dynamic

- response of underground box structure subjected to explosion seismic wave”, *Earthq. Struct.*, **8**(5), 1147-1170.
- Cui, Z., Sheng, Q. and Leng, X.L. (2016), “Control effect of a large geological discontinuity on the seismic response and stability of underground rock caverns: a case study of the Baihetan# 1 surge chamber”, *Rock Mech. Rock Eng.*, **49**(6), 2099-2114.
- Fattah, M.Y., Hamood, M.J. and Dawood, S.H. (2015), “Dynamic response of a lined tunnel with transmitting boundaries”, *Earthq. Struct.*, **8**(1), 275-304.
- Fattah, M.Y., Schanz, T. and Dawood, S.H. (2012), “The role of transmitting boundaries in modeling dynamic soil-structure interaction problems”, *Int. J. Eng. Technol.*, **2**(2), 236-258.
- Fu, X.D., Sheng, Q., Zhang, Y.H. and Dai, F. (2015), “Boundary setting method for the seismic dynamic response analysis of engineering rock mass structures using the discontinuous deformation analysis method”, *Int. J. Numer. Anal. Meth. Geomech.*, **39**(15), 1693-1712.
- Ge, X.R., Jiang, Y., Lu, Y.D. and Ren, J.X. (2010), “Testing study on fatigue deformation law of rock under cyclic loading”, *Chin. J. Rock Mech. Eng.*, **22**(10), 1581-1585.
- Grady, D.E. (1996), “Shock wave properties of brittle solids”, *AIP Conference Proceedings: Shock Compression of Condensed matters*, New York, May.
- Huang, H.X., Li, J., Rong, X.L., Fan, P.X. and Feng, S.F. (2016), “Dynamic response of underground box structure subjected to explosion seismic wave”, *Earthq. Struct.*, **10**(3), 669-680.
- Ismeik, M. and Shaqour, F. (2015), “Seismic lateral earth pressure analysis of retaining walls”, *Geomech. Eng.*, **8**(4), 523-540.
- Jafarnia, M. and Varzaghani, M.I. (2016), “Effect of near field earthquake on the monuments adjacent to underground tunnels using hybrid FEA-ANN technique”, *Earthq. Struct.*, **10**(4), 757-768.
- Ju, Q.H. and Wu, M.B. (1993), “Experimental studies on dynamic characteristics of rock under triaxial compression”, *Chin. J. Geotech. Eng.*, **15**(3), 73-80.
- Li, H. (2007), “Dynamic shearing constitutive model of lithologic material and application in finite element analysis”, Master Dissertation of Hohai University, Nanjing, China.
- Li, X.B., Zou, Y.J. and Ma, C.D. (2006), “Constitutive model of rock under coupled static-dynamic loading with intermediate strain rate”, *Chin. J. Rock Mech. Eng.*, **25**(5), 865-874.
- Lin, G., Chen, J.Y. and Xiao, S.Y. (2003), “Dynamic behavior of concrete and nonlinear seismic response of arch dam”, *J. Hydr. Eng.*, **34**(6), 30-36.
- Liu, J.B., Gu, Y. and Du, Y.X. (2007), “Consistent viscous-spring artificial boundaries and viscous-spring boundary elements”, *Chin. J. Geotech. Eng.*, **28**(9), 1070-1075.
- Mahmoud, S. (2014), “Blast load induced response and the associated damage of buildings considering SSI”, *Earthq. Struct.*, **7**(3), 349-365.
- Qi, C.Z., Miao, Q.S. and Qian, Q.H. (2002), “Dynamic model of rocks with consideration of strength-strain rate dependence”, *World Earthq. Eng.*, **18**(3), 52-56.
- Shang, J.L., Shen, L.T., Zhao, Y.H. and Zhao, J. (1998), “Dynamic constitutive equation of the Bukit Timah granite”, *Chin. J. Rock Mech. Eng.*, **17**(6), 634-641.
- Sun, J.Y. and Li, G.Q. (2006), “Development of solid material's constitutive model on the dynamic load”, *Sichuan Build. Sci.*, **32**(5), 144-149.
- The Professional Standards Compilation Group of the People's Republic of China (2015), “Code for seismic design of hydraulic structures of hydropower project (NB35047-2015)”, China Electric Power Press, Beijing, China.
- Xiao, M. (2000), “Mechanics of large long corridor of surge tank”, *Chin. J. Rock Mech. Eng.*, **19**(4), 476-480.
- Xiao, S.Y., Lin, G., Lu, J.Z. and Wang, Z. (2002), “Effect of strain rate on dynamic behavior of concrete in compression”, *J. Harbin Univ. C. E. & Arch.*, **35**(5), 35-39.
- Xiao, S.Y., Lin, G., Wang, Z. and Lu, J.Z. (2001), “Effect of strain rate on dynamic behavior of concrete in tension”, *J. Dalian Univ. Technol.*, **41**(6), 721-725.
- Xu, G., Chen, F. and Xiao, J.Q. (2005), “Experimental study of rock tensile strength under intermediate strain rate”, *Soil Eng. Found.*, **19**(4), 51-53.
- Yang, X.L. and Pan, Q.J. (2015), “Three dimensional seismic and static stability of rock slopes”, *Geomech. Eng.*, **8**(1), 97-111.
- Zhang, H. and Lu, F. (2009), “Test research on dynamic properties of granite under strain rate from 10^1 to 10^2s^{-1} ”, *Rock Soil Mech.*, **30**, 29-32.
- Zhang, Y.M. (2010), “Study on response characteristics of large underground cavern group under earthquake”, Doctoral Dissertation of Institute of Rock and Soil Mechanics, Chinese Academy of Sciences, Wuhan, China.
- Zhang, Y.T. (2011), “Study on seismic response analysis and structural plane-controlled stability of surrounding rock for large scale underground cavern complexes”, Doctoral Dissertation of Wuhan University, Wuhan, China.
- Zhang, Y.T., Xiao, M. and Chen, J.T. (2010), “Seismic damage analysis of underground caverns subjected to strong earthquake and assessment of post-earthquake reinforcement effect”, *Disast. Adv.*, **3**(4), 127-132.

CC